ACS SENSORS

Letter

pubs.acs.org/acssensors

Electrochemical Amplification in Side-by-Side Attoliter Nanogap Transducers

Hamid Reza Zafarani,[†] Klaus Mathwig,*[,‡] Ernst J. R. Sudhölter,[†] and Liza Rassaei*[,†]

[†]Laboratory of Organic Materials and Interfaces, Department of Chemical Engineering, Delft University of Technology, Van der Maasweg 9, 2629 HZ Delft, The Netherlands

[‡]University of Groningen, Groningen Research Institute of Pharmacy, Pharmaceutical Analysis, P.O. Box 196, 9700 AD Groningen, The Netherlands

Supporting Information

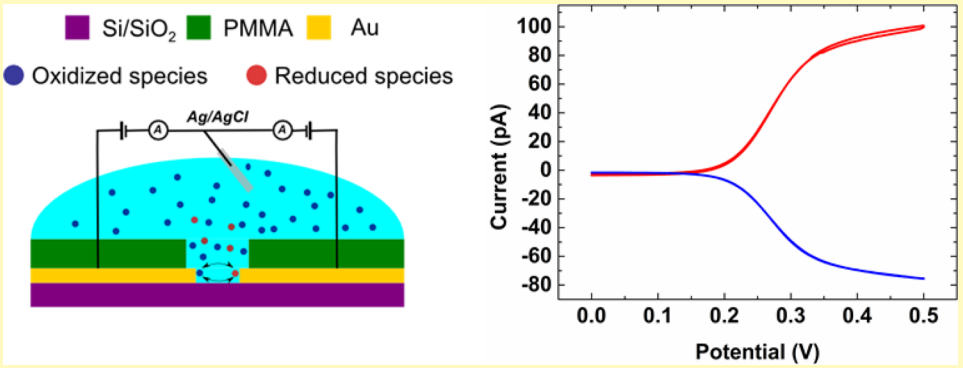

ABSTRACT: We report a strategy for the fabrication of a new type of electrochemical nanogap transducer. These nanogap devices are based on signal amplification by redox cycling. Using two steps of electron-beam lithography, vertical gold electrodes are fabricated side by side at a 70 nm distance encompassing a 20 attoliter open nanogap volume. We demonstrate a current amplification factor of 2.5 as well as the possibility to detect the signal of only 60 analyte molecules occupying the detection volume. Experimental voltammetry results are compared to calculations from finite element analysis.

KEYWORDS: *electrochemical sensor, generator-collector electrodes, nanofluidics, nanogap sensor, redox cycling, nanofabrication*

Demands for robust analysis at the clinical point-of-care[1,2] as well as for monitoring pollutants in the environment[3,4] have led to diverse research directions toward the development and further size reduction of miniaturized analytical chemical sensors. Electrochemical detectors combine the advantages of being sensitive tools with a low cost, small sample volume, and fast response time.[5−9] Here, progress stems from the developments in microfabrication techniques and their application in analytical chemistry.[10−14] Microelectrodes in particular offer a superior performance[15−18] with enhanced mass transport to the electrode surface resulting in a fast response time and often low detection limits and high signal-to-noise ratios.

The small surface areas of microelectrodes yield low currents, which are often difficult to detect with conventional electrochemical equipment.[19,20] An effective way for signal amplification is redox cycling, i.e., the successive oxidation and reduction of analyte molecules at two closely spaced electrodes. As analytes travel by diffusion between the electrodes, each molecule can shuttle up to thousands of times per second, leading to an intrinsic amplification of the current. In addition, in redox cycling only reversibly electrochemically active species yield an amplified signal and two separated working electrodes are employed, enabling biasing schemes for a highly selective sensing,[21,22] for example, by using interdigitated electrodes (IDEs).[16,23,24]

Microfabricated nanogap devices are a newer type of redox cycling devices which consist of two planar parallel electrodes closely spaced (≤100 nm) in a nanochannel, positioned as its bottom and ceiling in a thin-layer cell configuration;[25] or they can be realized as pore-based structures in which electrodes are stacked in vertical pores consisting of metal−insulator−metal layers.[26,27] Due to this small distance these devices can be employed for a variety of sensing schemes such as mesoscopic stochastic sensing, advanced biodetection, and single-molecule electrochemistry.[28−32] The fabrication of these devices requires several steps of consecutive electron-beam or photolithography, depositions, and dry etching, making the overall process rather complex.

Here, we report a novel nanogap transducer which we had previously investigated by numerical methods.[33] The geometry consists of two electrodes positioned side by side at a 70 nm

Received: March 22, 2017
Accepted: May 16, 2017
Published: May 16, 2017

DOI: 10.1021/acssensors.7b00180
ACS Sens. 2017, 2, 724−728

distance. The electrode pair is not covered to form a closed nanochannel, but the active detection volume is directed to a larger reservoir. The active volume is 20 attoliters, about 100 times less than previously reported for closed nanogap devices.[28] Our device resembles an interdigitated electrode array[16,34,35] with several unique properties: it only has two fingers; the nanoscale interelectrode distance is considerably smaller than in most IDEs;[36−38] the electrode surfaces are parallel[39] and are passivated on top. We characterized the device by cyclic voltammetry and step amperometry to determine the amplification factor, sensitivity, and time response, and compared the experimental performance by two-dimensional finite element analysis.

EXPERIMENTAL SECTION

Device Fabrication. Two steps of electron-beam lithography were employed to pattern devices on a silicon wafer substrate passivated by 300 nm thermally grown silicon oxide. Figure 1A shows the fabrication

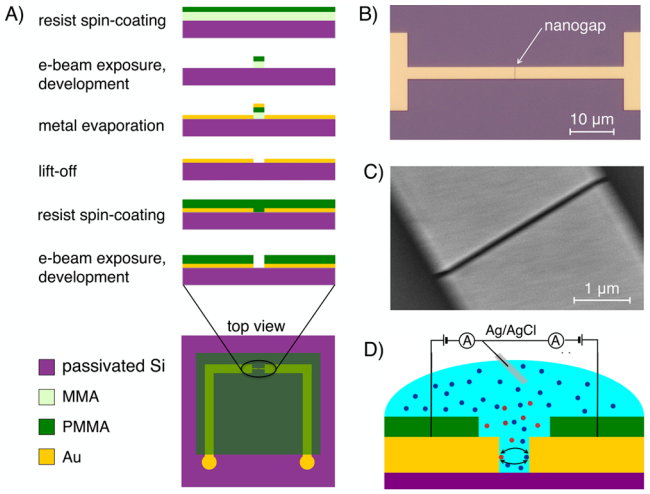

Figure 1. (A) Schematic of the nanogap fabrication process. (B) Microscopic top view image of a typical nanogap device. (C) Electron micrograph of the Au-PMMA nanogap. (D) Schematic principle of electrochemical measurements.

scheme. First, two layers of methyl methacrylate (MMA) and poly(methyl methacrylate) (PMMA) (thicknesses of 300 and 150 nm) were successively spin-coated on the substrate. Two 3-μm-wide electrodes with a 70 nm gap in between were patterned by e-beam exposure. Next, a 10-nm-thick Ti adhesion layer and 80-nm-thick Au were deposited by electron-beam evaporation, followed by a lift-off (hence, active volume = 3 μm × 70 nm × 80 nm ≈ 20 attoliters). Subsequently, a 500-nm-thick PMMA passivation layer was spin-coated. In a second e-beam exposure and development step, only the gap area and connection pads were exposed. Microscopic top-view images of a nanogap (Au and passivation layer) are shown in Figure 1B and C.

Chemicals. 1,1-Ferrocenedimethanol, $Fc(MeOH)_2$, and potassium chloride, KCl, were obtained from Sigma-Aldrich. All solutions were freshly prepared in Milli-Q water with 1 M KCl as supporting electrolyte. The experiments were carried out at room temperature.

Electrochemical Experiments. A Keithley 4200 parameter analyzer with two source measurement units was used to separately bias both electrodes as well as to measure Faradaic currents. A Ag/AgCl reference electrode (BASi Inc.) was positioned in a reservoir on top of the nanogap device. Figure 1D shows the measurement setup.

RESULTS AND DISCUSSION

Fabrication of the Nanogap. Focused ion beam milling has been employed for the fabrication of the nanogaps for single molecule measurements in the field of molecular electronics,[40−42] and it has the advantage of fabrication in a single milling step. However, we found that this technique is not optimally suited for our nanogaps: due to the Gaussian distribution of the ion beam, v-shaped nanogap structures were obtained instead of parallel straight walls.[40,43,44] Moreover, by employing ion beam milling, not only the metal but also the passivation layer around the gap are removed (with a Gaussian geometry); hence surrounding the gap a large area of the electrodes remains bare without any passivation on top.

Using e-beam lithography and lift-off, well-defined clean sidewalls of two closely spaced electrodes are more easily achievable. While we chose a gap width of 70 nm, also considerably shorter interelectrode distances are feasible (possibly at reduced metal thicknesses). Moreover, using this fabrication by deposition, lithography, and lift-off, electrodes can be fabrication in a large variety of materials. A second e-beam exposure defined the insulating layer; to avoid covering the nanogap with PMMA due to misalignment, a wider opening was chosen (50 nm tolerance). While this layer does not allow the use of organic solvent in electrochemical measurements, it can be replaced by inert materials such as silicon oxide.

Current Amplification. We compared the current of the nanogap transducers in single mode (i.e., biasing only one electrode) and in redox cycling dual mode to determine the amplification factor. Figure 2 presents cyclic voltammograms

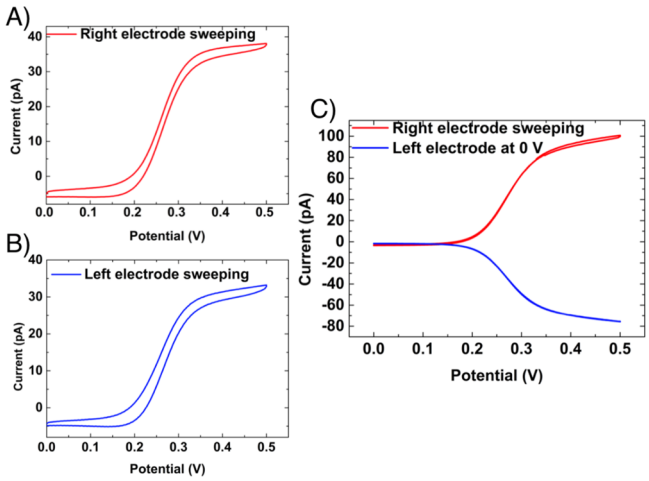

Figure 2. Cyclic voltammograms of 0.5 mM $Fc(MeOH)_2$ in 1 M KCl solution in the nanogap at a 5 mV s^{-1} scan rate. (A) The right electrode was swept between 0 to 0.5 V (vs Ag/AgCl) while the left electrode was disconnected. (B) The left electrode was swept between 0 and 0.5 V while the right electrode was disconnected. (C) The right electrode was swept between 0 and 0.5 V while the left electrode was kept constant at 0 V.

for a device filled with 0.5 mM $Fc(MeOH)_2$ in a 1 M KCl aqueous solution. In single mode (see Figure 2A,B), the potential of one electrode was swept while the other one was kept floating. In dual mode (see Figure 2C), one electrode was swept (right generator electrode) from 0 to 0.5 V while the left collector electrode was kept at a constant reducing potential of 0 V vs Ag/AgCl. Comparing the limiting currents in single mode, I_{single}, and dual mode, I_{dual}, leads to an amplification

DOI: 10.1021/acssensors.7b00180
ACS Sens. 2017, 2, 724−728

factor of I_{dual}/I_{single} = 2.5. The difference between the limiting currents of the right and left electrodes (100 pA vs 75 pA at 0.5 V) in Figure 3C stems from the open geometry of the

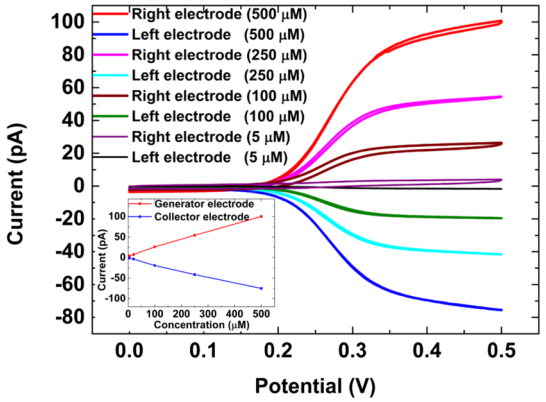

Figure 3. Cyclic voltammograms of different concentrations of $Fc(MeOH)_2$ in 1 M KCl solution at a 5 mV s^{-1} scan rate. Inset: Limiting current at 0.5 V as a function of concentration: 5, 10, 100, 250, and 500 μM (lines are guides for the eye).

nanogap; oxidized and reduced species produced at one electrode can diffuse back into the solution before reaching the next electrode. Thus, amplification factor and collection efficiency are reduced, and a collection efficiency of $I_{collector}/I_{generator}$ = 75% was obtained.

The Faradaic limiting current for two planar opposing electrodes is determined as[22]

$$I = \frac{nFADC}{z} \quad (1)$$

where n is the number of exchanged electrons, F the Faraday constant, A the electrode surface area, D the diffusion coefficient, C the analyte concentration, and z the interelectrode distance. Using eq 1 yields a current of I = 110 pA in good agreement with the experimental value of 100 pA. The effective redox cycling volume in between the two electrodes amounts to 20 aL, which is about 100 times smaller than in smallest electrochemical nanochannel sensors.[28,45,46]

Concentration Effect: Detection Limit. In order to quantitatively investigate the detection limit of the nanogap transducers, we performed cyclic voltammetry for different concentrations of $Fc(MeOH)_2$ in 1 M KCl solution as presented in Figure 3. The right electrode potential was swept between 0 and 0.5 V (at a 5 mV s^{-1} scan rate) while the left electrode was fixed at 0 V. Well-defined cyclic voltammograms were obtained for $Fc(MeOH)_2$ concentrations down to 5 μM, showing in linear response in the limiting current (see inset in Figure 3). For the concentration of 5 μM, corresponding to an average number of 60 molecules in the active volume, a limiting current of 1.5 pA was measured at the collector electrode. (Lower concentrations were inaccessible due to an instrumental limitation of 1 pA.)

Response Time. The response time is an important characteristic of nanogap sensors;[47] it is the time to reach a steady-state current after a change in concentration (or a change in local concentration induced by stepping an electrode potential). In closed nanochannels, molecules have to diffuse from the bulk and through the access holes *along* the entire nanochannel (length L) to reach an equilibrium concentration. The response time $\tau \propto L^2/D$ is further slowed down by reversible potential-dependent adsorption of analytes and can amount to several tens of seconds.[47,48]

We investigated the response time of the side-by-side devices by stepping the potential of one of the electrodes between 0 and 0.5 V and observing the current response at the other electrode biased constantly at 0 V (see Figure 4). While the

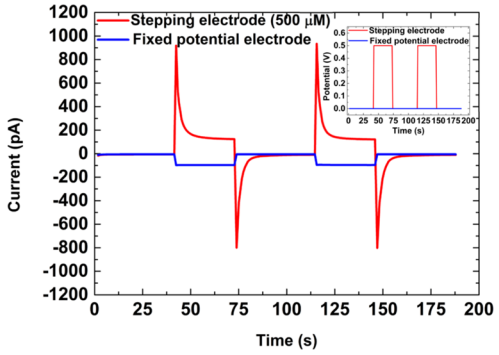

Figure 4. Step chronoamperometry for 0.5 mM $Fc(MeOH)_2$ in 1 M KCl solution. The left electrode (blue) is kept at a constant potential of 0 V; the right electrode (red) is stepped to either 0 or 0.5 V. Inset: applied potentials as a function of time.

stepping electrode exhibits considerable transient behavior due to parasitic *RC* charging,[47] the collector electrode shows an instant response, limited by the instrumental time resolution of 0.2 s. We estimate that the actual response time of the device is much shorter, as it only takes $\propto 80\ nm^2/D$ = 10 μs to diffuse into its active area. Also, moderately fast sweeping in cyclic voltammetry without hysteresis is facilitated due to this fast response (see Supporting Information for scan rates ranging from 1 to 40 mV s^{-1}).

Numerical Analysis. We employed two-dimensional finite element analysis (COMSOL Multiphysics 4.4; see Supporting Information) to model the electrochemical reactions in the nanogap, following up our previous, more detailed numerical investigation of the effect of several geometric parameters on redox cycling in the side-by-side nanogap geometry.[33] Numerically and experimentally obtained cyclic voltammograms for 0.5 mM $Fc(MeOH)_2$ in 1 M KCl at 5 mV s^{-1} are compared in Figure 5 (a 50 nm tolerance of PMMA layer is considered in

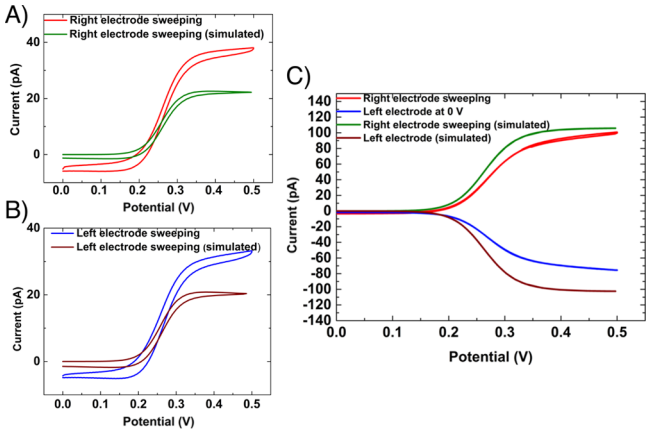

Figure 5. Comparison of simulated and experimental cyclic voltammograms obtained for 0.5 mM $Fc(MeOH)_2$ in 1 M KCl solution at a 5 mV s^{-1} scan rate for (A,B) single mode and (C) redox cycling.

DOI: 10.1021/acssensors.7b00180
ACS Sens. 2017, 2, 724−728

the simulation as well). There is good agreement with the experimental voltammograms slightly deviating higher potentials in redox cycling, presumably due to slower electron transfer kinetics, and exhibiting lower limiting currents. In redox cycling, the current is 5% lower for the generator electrode and 26% lower for the collector electrode with respect to the numerical values (at 0.5 V; see Figure 5C). We attribute these differences to deviations of the device geometry (electrode height and distance, alignment of passivation layer) from nominal values, as well as by the fact that generated molecules can escape the nanogap at both ends, which is not captured by the 2D simulation. For the same reason of a 3D electrode, in single mode the 2D simulation yields lower current values (see Figures 5A,B), leading to a high numerical amplification factor of 5. Compared to our previous simulation[33] (factor of 8) this amplification factor is lower because we take the wider opening of the passivation layer into account.

CONCLUSIONS

We developed a new electrochemical nanogap transducer geometry by placing two electrodes side by side at a 70 nm distance. Fabrication comprises only two lithography steps and makes it possible to fabricate a wide range of gap sizes and make use of different electrode materials, i.e., any material that can be sputtered or deposited.

While our open geometry enables a very fast response time compared to covered nanogaps, this comes at the cost of a reduced amplification factor and a short residence time of individual molecules between the electrodes. Thus, it is currently not possible to perform single-molecule detection or mesoscopic sensing as is possible in covered nanochannel sensors.

We are convinced that—next to the shown advantages of ease of fabrication and the possible variation of electrode materials—our devices will realize their full potential in future planned experiments for three reasons: First, the nanogap can be covered (e.g., with a glass coverslip) enclosing a 20−100 aL nanochannel volume (depending of the channel length), which is at least 1 order of magnitude smaller than previously reported nanogap channels.[30] Such small volumes make single molecule detection come into reach. Second, the side-by-side arrangement allows direct access of optical detection methods either from the top or through a transparent substrate using an inverted microscope, thus enabling direct observation of combined optical−electrochemical molecular properties.[49] Third, e-beam lithography allows a further considerable reduction of the interelectrode distance, increasing its sensitivity and further reducing the active volume. Therefore, we anticipate that the side-by-side nanogap transducers will form a versatile nanoscale electroanalytical tool.

ASSOCIATED CONTENT

Supporting Information

The Supporting Information is available free of charge on the ACS Publications website at DOI: 10.1021/acssensors.7b00180.

Effect of scan rate; Numerical methods (PDF)

AUTHOR INFORMATION

Corresponding Authors

*E-mail: k.h.mathwig@rug.nl.

*E-mail: l.rassaei@tudelft.nl.

ORCID

Klaus Mathwig: 0000-0002-8532-8173

Ernst J. R. Sudhölter: 0000-0003-3296-953X

Notes

The authors declare no competing financial interest.

REFERENCES

(1) Cruz, A. F. D.; Norena, N.; Kaushik, A.; Bhansali, S. A low-cost miniaturized potentiostat for point-of-care diagnosis. *Biosens. Bioelectron.* **2014**, *62*, 249−254.

(2) Mathwig, K.; Albrecht, T.; Goluch, E. D.; Rassaei, L. Challenges of biomolecular detection at the nanoscale: nanopores and microelectrodes. *Anal. Chem.* **2015**, *87* (11), 5470−5475.

(3) Omanović, D.; Garnier, C.; Gibbon−Walsh, K.; Pižeta, I. Electroanalysis in environmental monitoring: Tracking trace metals—A mini review. *Electrochem. Commun.* **2015**, *61*, 78−83.

(4) Wang, N.; Kanhere, E.; Miao, J.; Triantafyllou, M. S. Miniaturized chemical sensor with bio-inspired micropillar working electrode array for lead detection. *Sens. Actuators, B* **2016**, *233*, 249−256.

(5) Ben-Yoav, H.; Dykstra, P. H.; Bentley, W. E.; Ghodssi, R. A microfluidic-based electrochemical biochip for label-free diffusion-restricted DNA hybridization analysis. *Biosens. Bioelectron.* **2012**, *38* (1), 114−120.

(6) Demchenko, A. P. The sensing devices, in *Introduction to Fluorescence Sensing*; Springer, 2015; pp 507−550.

(7) Ríos, Á.; Zougagh, M.; Avila, M. Miniaturization through lab-on-a-chip: Utopia or reality for routine laboratories? A review. *Anal. Chim. Acta* **2012**, *740*, 1−11.

(8) Chang, F.; Xie, X.; Li, M.; Zhu, Z. A miniaturized electrochemical device integrating a biconical microchannel and carbon fiber disk ultramicroelectrode. *Analyst* **2016**, *141* (16), 4859−4862.

(9) Zhu, X.; Ahn, C. H. On-chip electrochemical analysis system using nanoelectrodes and bioelectronic CMOS chip. *IEEE Sens. J.* **2006**, *6* (5), 1280−1286.

(10) Wang, J. Electrochemical detection for microscale analytical systems: a review. *Talanta* **2002**, *56* (2), 223−231.

(11) Oja, S. M.; Wood, M.; Zhang, B. Nanoscale electrochemistry. *Anal. Chem.* **2013**, *85* (2), 473−486.

(12) Kanno, Y.; Ino, K.; Shiku, H.; Matsue, T. A local redox cycling-based electrochemical chip device with nanocavities for multi-electrochemical evaluation of embryoid bodies. *Lab Chip* **2015**, *15* (23), 4404−4414.

(13) Rackus, D. G.; Shamsi, M. H.; Wheeler, A. R. Electrochemistry, biosensors and microfluidics: a convergence of fields. *Chem. Soc. Rev.* **2015**, *44* (15), 5320−5340.

(14) Mathwig, K.; Chi, Q.; Lemay, S. G.; Rassaei, L. Handling and sensing of single enzyme molecules: from fluorescence detection towards nanoscale electrical measurements. *ChemPhysChem* **2016**, *17*, 452−457.

(15) Montenegro, M.; Queiros, A.; Daschbach, J. *Microelectrodes—Principles and Applications*; NATO ASI Series (2nd ed.); Reidel: Dordrecht, 1990.

(16) Alayo, N.; Fernández-Sánchez, C.; Baldi, A.; Esquivel, J. P.; Borrisé, X.; Pérez-Murano, F. Gold interdigitated nanoelectrodes as a sensitive analytical tool for selective detection of electroactive species via redox cycling. *Microchim. Acta* **2016**, *183* (5), 1633−1639.

(17) Ronkainen, N. J., Micro-and Nanoelectrodes in Protein-Based Electrochemical Biosensors for Nanomedicine and Other Applications. In *Advanced Bioelectronics Materials*, 2015; p 1; DOI: 10.1002/9781118998861.ch1.

(18) Gross, A. J.; Marken, F. *ITO-ITO Dual-Plate Microgap Electrodes: E and EC′ Generator-Collector Processes*. *Electroanalysis* **2015**, *27* (4), 1035−1042.

(19) Vagin, M. Y.; Sekretaryova, A. N.; Reategui, R. S.; Lundstrom, I.; Winquist, F.; Eriksson, M. Arrays of Screen-Printed Graphite Microband Electrodes as a Versatile Electroanalysis Platform. *ChemElectroChem* **2014**, *1* (4), 755−762.

DOI: 10.1021/acssensors.7b00180
ACS Sens. 2017, 2, 724−728

(20) Compton, R. G.; Wildgoose, G. G.; Rees, N. V.; Streeter, I.; Baron, R. Design, fabrication, characterisation and application of nanoelectrode arrays. *Chem. Phys. Lett.* **2008**, *459* (1), 1−17.
(21) Zafarani, H. R.; Mathwig, K.; Lemay, S. G.; Sudhölter, E. J.; Rassaei, L. Modulating selectivity in nanogap sensors. *ACS Sensors* **2016**, *1* (12), 1439−1444.
(22) Goluch, E. D.; Wolfrum, B.; Singh, P. S.; Zevenbergen, M. A.; Lemay, S. G. Redox cycling in nanofluidic channels using interdigitated electrodes. *Anal. Bioanal. Chem.* **2009**, *394* (2), 447−456.
(23) Morita, M.; Hayashi, K.; Horiuchi, T.; Shibano, S.; Yamamoto, K.; Aoki, K. J. Enhancement of Redox Cycling Currents at Interdigitated Electrodes with Elevated Fingers. *J. Electrochem. Soc.* **2014**, *161* (4), H178−H182.
(24) Ueno, K.; Hayashida, M.; Ye, J.-Y.; Misawa, H. Fabrication and electrochemical characterization of interdigitated nanoelectrode arrays. *Electrochem. Commun.* **2005**, *7* (2), 161−165.
(25) Zevenbergen, M. A.; Krapf, D.; Zuiddam, M. R.; Lemay, S. G. Mesoscopic concentration fluctuations in a fluidic nanocavity detected by redox cycling. *Nano Lett.* **2007**, *7* (2), 384−388.
(26) Fu, K.; Han, D.; Ma, C.; Bohn, P. W. Electrochemistry at single molecule occupancy in nanopore-confined recessed ring-disk electrode arrays. *Faraday Discuss.* **2016**, *193*, 51−64.
(27) Han, D.; Zaino, L. P., III; Fu, K.; Bohn, P. W. Redox Cycling in Nanopore-Confined Recessed Dual-Ring Electrode Arrays. *J. Phys. Chem. C* **2016**, *120* (37), 20634−20641.
(28) Rassaei, L.; Mathwig, K.; Kang, S.; Heering, H. A.; Lemay, S. G. Integrated biodetection in a nanofluidic device. *ACS Nano* **2014**, *8* (8), 8278−8284.
(29) Singh, P. S.; Lemay, S. G. Stochastic Processes in Electrochemistry. *Anal. Chem.* **2016**, *88* (10), 5017−5027.
(30) Kang, S.; Nieuwenhuis, A. F.; Mathwig, K.; Mampallil, D.; Kostiuchenko, Z. A.; Lemay, S. G. Single-molecule electrochemistry in nanochannels: probing the time of first passage. *Faraday Discuss.* **2016**, *193*, 41−50.
(31) Mathwig, K.; Zafarani, H. R.; Speck, J. M.; Sarkar, S.; Lang, H.; Lemay, S. G.; Rassaei, L.; Schmidt, O. G. Potential-Dependent Stochastic Amperometry of Multiferrocenylthiophenes in an Electrochemical Nanogap Transducer. *J. Phys. Chem. C* **2016**, *120* (40), 23262−23267.
(32) Mathwig, K.; Lemay, S. G. Pushing the limits of electrical detection of ultralow flows in nanofluidic channels. *Micromachines* **2013**, *4* (2), 138−148.
(33) Zafarani, H. R.; Mathwig, K.; Sudhölter, E. J.; Rassaei, L. Electrochemical redox cycling in a new nanogap sensor: design and simulation. *J. Electroanal. Chem.* **2016**, *760*, 42−47.
(34) Azizah, N.; Hashim, U.; Gopinath, S. C.; Nadzirah, S. Gold nanoparticle mediated method for spatially resolved deposition of DNA on nano-gapped interdigitated electrodes, and its application to the detection of the human Papillomavirus. *Microchim. Acta* **2016**, *183* (12), 3119−3126.
(35) Zhu, X.; Ahn, C. H. Electrochemical determination of reversible redox species at interdigitated array micro/nanoelectrodes using charge injection method. *IEEE Trans. Nanobiosci.* **2005**, *4* (2), 164−169.
(36) Shim, J. S.; Rust, M. J.; Ahn, C. H. A large area nano-gap interdigitated electrode array on a polymer substrate as a disposable nano-biosensor. *J. Micromech. Microeng.* **2013**, *23* (3), 035002.
(37) Hayashi, K.; Takahashi, J.-i.; Horiuchi, T.; Iwasaki, Y.; Haga, T. Development of nanoscale interdigitated array electrode as electrochemical sensor platform for highly sensitive detection of biomolecules. *J. Electrochem. Soc.* **2008**, *155* (9), J240−J243.
(38) Skjolding, L.; Spegel, C.; Ribayrol, A.; Emnéus, J.; Montelius, L. Characterisation of nano-interdigitated electrodes. In *Journal of Physics: Conference Series*; IOP Publishing, 2008.
(39) Kamath, R. R.; Madou, M. J. Three-Dimensional Carbon Interdigitated Electrode Arrays for Redox-Amplification. *Anal. Chem.* **2014**, *86* (6), 2963−2971.
(40) Nagase, T. Nano-gap Electrodes Developed Using Focused Ion Beam Technology. In *Handbook of Manufacturing Engineering and Technology*; Springer, 2015; pp 1513−1528.
(41) Nagase, T.; Kubota, T.; Mashiko, S. Fabrication of nano-gap electrodes for measuring electrical properties of organic molecules using a focused ion beam. *Thin Solid Films* **2003**, *438*, 374−377.
(42) Purohit, G.; Shankar, M.; Gupta, D.; Damodaran, S.; Katiyar, M. Fabrication of nano-gap electrodes using a focused ion beam for measuring electrical properties of molecular scale transistors; 16th International Workshop on Physics of Semiconductor Devices, 2012. DOI: 10.1117/12.928079.
(43) Young, R.; Cleaver, J.; Ahmed, H. Characteristics of gas-assisted focused ion beam etching. *J. Vac. Sci. Technol., B: Microelectron. Process. Phenom.* **1993**, *11* (2), 234−241.
(44) Tseng, A. A. Recent developments in micromilling using focused ion beam technology. *J. Micromech. Microeng.* **2004**, *14* (4), R15.
(45) Zevenbergen, M. A.; Wolfrum, B. L.; Goluch, E. D.; Singh, P. S.; Lemay, S. G. Fast electron-transfer kinetics probed in nanofluidic channels. *J. Am. Chem. Soc.* **2009**, *131* (32), 11471−11477.
(46) Rassaei, L.; Mathwig, K.; Goluch, E. D.; Lemay, S. G. Hydrodynamic voltammetry with nanogap electrodes. *J. Phys. Chem. C* **2012**, *116* (20), 10913−10916.
(47) Kang, S.; Mathwig, K.; Lemay, S. G. Response time of nanofluidic electrochemical sensors. *Lab Chip* **2012**, *12* (7), 1262−1267.
(48) Mampallil, D.; Mathwig, K.; Kang, S.; Lemay, S. G. Reversible adsorption of outer-sphere redox molecules at Pt electrodes. *J. Phys. Chem. Lett.* **2014**, *5* (3), 636−640.
(49) Al-Kutubi, H.; Zafarani, H. R.; Rassaei, L.; Mathwig, K. Electrofluorochromic systems: molecules and materials exhibiting redox-switchable fluorescence. *Eur. Polym. J.* **2016**, *83*, 478−498.

DOI: 10.1021/acssensors.7b00180
ACS Sens. 2017, 2, 724−728